J. Fluid Mech. (1986), *vol.* 165, *pp.* 231–246
Printed in Great Britain

An integral method for subcritical compressible flow

By M. G. HILL, N. RILEY
School of Mathematics and Physics, University of East Anglia, Norwich NR4 7TJ
AND K. W. MORTON
Oxford University Computing Laboratory, Oxford OX1 3QD

(Received 24 June 1985)

The boundary-integral, or panel, method of solution of the plane potential-flow equation for incompressible flow is well established. We extend the method to the fully compressible problem, in subcritical flow conditions. The method is applied to single- and to multi-element configurations.

1. Introduction

In a recent (Hill 1983) and a forthcoming (Hill & Porter 1986) publication a method for determining the fundamental solution of a general two-dimensional elliptic partial differential equation is addressed, in terms of which particular solutions may be represented. We exploit the technique in this paper to develop solutions of the full two-dimensional potential equation, in subcritical flow conditions, for the flow past a multi-element high-lift wing. Such a configuration may contain as many as four elements, and even at modest free-stream speeds compressibility effects may not be negligible; indeed the flow over the forward part of the slat may be supercritical. Our approach results in a boundary-integral or panel method for the solution of the full two-dimensional potential equation in steady flow past a multi-element configuration in subcritical flow conditions.

Panel methods of solution of the incompressible potential equation are effective, flexible and well established; see Hess & Smith (1966), Hess (1973). In such a method the solution is represented by a distribution of sources and/or vortices over the bounding surfaces of the flow. Application of the boundary conditions leads to a Fredholm integral equation that has to be solved for the source/vortex strengths. The solution of this integral equation is effected by a suitable discretization of the boundary and choice of singularity distributions. Since, unlike finite-difference methods of solution of the governing equation, the method does not require the generation of a computation mesh, the calculation of the flow past a multi-element configuration presents no more difficulty than a single aerofoil. In this paper we show that a compressible analogue of the familiar panel method may be constructed. The method differs significantly from the so-called field-panel methods (see, for example, Oskam 1985). In these methods terms in the potential equation that are associated with compressibility effects are treated as distributed source terms. This enables the use of incompressible-flow panel methods with the expression for the potential now containing an additional double field integral whose integrand involves the unknown potential.

The plan of the present paper is as follows. In §2 we formulate the nonlinear

problem, and outline schematically the iterative method that is proposed for its solution. This is followed in §3 by a description of the panel method that we propose to adopt, as applied to incompressible flow. In §4 we address the full compressible problem. A key feature in its solution is the derivation of the fundamental solution of the linearized potential equation, which is a part of the iterative scheme, via a Volterra integral equation. The solution of this equation allows us to construct the analogue of the source/vorticity distribution, for incompressible flow, in the Fredholm integral equation. The convergence of our iterative method of solution is established in §5. Finally, in §6 we present results for subcritical flow past a variety of configurations involving one or more elements. A comparison with the results obtained by other authors establishes the effectiveness of the method. Its flexibility and power become apparent as the number of elements in the configuration increases. Apart from additional computer time, the method is independent of the number of elements in the configuration.

2. Problem formulation

We are concerned with the steady, two-dimensional flow of an inviscid, compressible fluid past one or more shapes of aerodynamic interest. We make the assumptions that the fluid is a perfect gas, that the flow is irrotational and, for the subcritical flows under consideration here, that the flow is isentropic.

If the uniform fluid speed and density at infinity, U_1 and ρ_1, are taken as reference speed and density respectively, and a typical dimension l of a body in the flow field as a reference length, then with $\boldsymbol{v} = (u, v) = \boldsymbol{\nabla}\Phi$ the equation satisfied by the potential Φ is, in a Cartesian co-ordinate system (x, y),

$$\frac{\partial}{\partial x}\left(\rho\frac{\partial \Phi}{\partial x}\right)+\frac{\partial}{\partial y}\left(\rho\frac{\partial \Phi}{\partial y}\right) = 0. \tag{2.1}$$

Using the isentropic relation $a^2 = \rho^{\gamma-1}$, where a is the speed of sound made dimensionless with its value at infinity a_1, and γ is the ratio of the specific heats, the energy integral of the governing equations, or Bernoulli equation, may be written as

$$\rho = \{1+\tfrac{1}{2}(\gamma-1)\,M_1^2(1-q^2)\}^{1/(\gamma-1)} = B(\Phi), \tag{2.2}$$

where $q^2 = u^2+v^2 = |\boldsymbol{\nabla}\Phi|^2$, and $M_1 = U_1/a_1$ is the free-stream Mach number.

The equations (2.1) and (2.2) are to be solved subject to the boundary conditions

$$\Phi \sim x \quad \text{as } |\boldsymbol{x}|\to\infty, \quad \boldsymbol{\nabla}\Phi\cdot\boldsymbol{n} = 0 \quad \text{on } C, \tag{2.3a,b}$$

where we have assumed that the flow at infinity is parallel to the x-axis, and taken $\boldsymbol{n}$ as the unit normal to an internal boundary C of it. In addition to (2.3) we apply a Kutta condition at the sharp trailing edge of each of the aerodynamic shapes that bound the flow internally. In this way the circulation about each shape is determined and the solution rendered unique.

Since (2.1) and (2.2) are nonlinear we have adopted an iterative solution method which is represented schematically as

$$\boldsymbol{\nabla}\cdot(\rho^i\,\boldsymbol{\nabla}\Phi^{i+1}) = 0, \quad \rho^i = B(\Phi^i), \tag{2.4a,b}$$

where a superscript i denotes the ith iterate. Thus, at each stage of the iteration the partial differential equation to be solved, namely (2.4a), is a linear equation. If we write (2.1) as

$$\frac{\partial^2\Phi}{\partial x^2}+\frac{\partial^2\Phi}{\partial y^2}+\frac{\partial}{\partial x}(\log\rho)\frac{\partial\Phi}{\partial x}+\frac{\partial}{\partial y}(\log\rho)\frac{\partial\Phi}{\partial y} = 0, \tag{2.5}$$

then the problem to be solved, with $\rho = \rho(x, y)$ assumed known, is the linear second-order partial differential equation with variable coefficients (2.5), subject to (2.3) and appropriate Kutta conditions. In the next section we introduce the solution method for the special case $\rho \equiv 1$, and in §4 show how the method may be extended to fully compressible flows.

3. Incompressible flow

When $M_1 = 0$ we have $\rho = 1$, and our basic equation (2.5) reduces to the familiar plane Laplace equation

$$\frac{\partial^2 \Phi}{\partial x^2} + \frac{\partial^2 \Phi}{\partial y^2} = 0, \tag{3.1}$$

for incompressible flow. This equation is to be solved subject to (2.3) and appropriate Kutta conditions.

For single aerofoils exact solutions of the problem posed by (3.1), and its boundary conditions, are available from conformal-transformation methods in which the body is transformed to a circle. Williams (1973) has also used this method for two lifting aerofoils by transforming them to two circles between which there are multiple reflections of the doublet and vortex singularities contained within them. Suddhoo (1985) has shown how Williams' method can be extended to multi-element aerofoils and presents examples for configurations with three and four elements.

In the present paper our method of solution is based upon the boundary-integral or panel method, in which the solution is represented by a distribution of singularities over the bounding surfaces. This method, which is capable of computational accuracy comparable with that of the methods described above, has found wide acceptance within the aerodynamics community. For a general account of these methods reference may be made to the work of Hess & Smith (1966) and Hess (1973). The method is flexible and, as demonstrated in §4 below, can be extended to multi-element configurations in compressible flow with little extra computational effort.

To implement such a method of solution we first note that the fundamental solution of (3.1) and its conjugate harmonic function may be written as

$$\left.\begin{aligned} \log R &= \tfrac{1}{2} \log\{(x-\xi)^2 + (y-\eta)^2\}, \\ \theta &= \tan^{-1}\left[\frac{y-\eta}{x-\xi}\right]. \end{aligned}\right\} \tag{3.2}$$

These correspond to the potentials of a line source and a line vortex respectively, and the solution of (3.1) may be constructed formally, as distributions of such singularities over the bounding surfaces, as

$$\Phi(\boldsymbol{p}) = \Phi_\infty(\boldsymbol{p}) + \int_C \sigma(\boldsymbol{q}) \log|\boldsymbol{p}-\boldsymbol{q}| \, \mathrm{d}q + \int_C \gamma(\boldsymbol{q})\, \theta(\boldsymbol{p}-\boldsymbol{q}) \, \mathrm{d}q, \tag{3.3}$$

where $\boldsymbol{p} = (x, y)$ is the point at which Φ is evaluated, $\boldsymbol{q} = (\xi, \eta)$ is a point on the boundary C, with which $\boldsymbol{p}$ does not coincide, $\Phi_\infty(\boldsymbol{p}) = x$, and the source and vortex strengths σ and γ are to be determined. In the method that we use, which originated with British Aerospace (see Newling 1977), we retain distributions of both sources and vortices; the former essentially account for the aerofoil thickness whilst the latter deal with the lift. The source and vortex strengths are determined from the solution of an integral equation that is derived from (2.3*b*), and the normal derivative of (3.3), when $\boldsymbol{p}$ is taken on the boundary C, which is

$$\frac{\partial}{\partial n_p}\Phi(\boldsymbol{p}) = \frac{\partial}{\partial n_p}\Phi_\infty(\boldsymbol{p}) + \pi\sigma(\boldsymbol{p}) + \int_C \sigma(\boldsymbol{q}) \frac{\partial}{\partial n_p} \log|\boldsymbol{p}-\boldsymbol{q}| \, \mathrm{d}q + \int_C \gamma(\boldsymbol{q}) \frac{\partial}{\partial n_p}\theta(\boldsymbol{p}-\boldsymbol{q}) \, \mathrm{d}q, \tag{3.4}$$

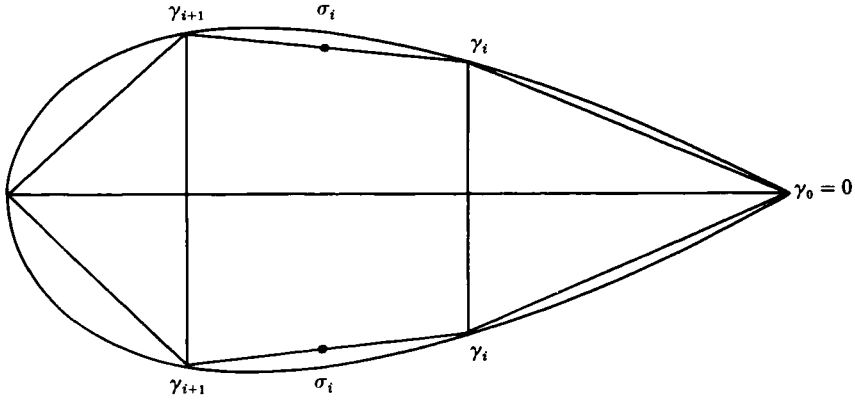

FIGURE 1. Discretization of the bounding curve C.

where $\partial/\partial n_p$ denotes the derivative normal to the boundary C at the point $\boldsymbol{p}$. (The resolution of the apparent indeterminacy associated with this procedure is discussed below.) In order to solve (2.3b), (3.4) for the source and vortex strengths σ and γ, the boundary C, which may consist of one or more elements, is discretized so that it is represented by a sequence of boundary elements or 'panels'. These panels may be straight-line, circular-arc or higher-order segments as discussed by Hess (1973). In this paper we choose straight-line segments and, with reference to an aerodynamic shape, we represent each of the upper and lower surfaces by N such panels, making $2N$ panels in all. The panels may vary in length, and may be constructed in a variety of ways. However, since we wish to identify corresponding panels on the upper and lower surfaces, we divide the straight line joining the nose and the trailing edge into N, not necessarily equal, segments and take as our panels the linear projections of these on to C as in figure 1. The form of the distributions for σ and γ must also be specified. The source strength is taken as piecewise constant so that $\sigma = \sigma_i$ on the ith panel, and the vorticity distribution is taken to be a continuous, piecewise-linear function. Thus, over the ith panel $\gamma = \gamma_{i-1} + (\gamma_i - \gamma_{i-1})\, s$, where $0 \leqslant s \leqslant 1$ along the panel and γ_{i-1}, γ_i represent the vortex strengths at each end of it. Finally, if a sharp trailing edge corresponds to $i = 0$ we set $\gamma_0 = 0$ to satisfy the Kutta condition. The boundary condition (2.3b) is now satisfied, using the discretized form of (3.4) obtained by evaluating the integrals numerically over all the panels into which C has been divided, at the $2N$ nodal points that are defined to be the panel mid-points. This provides us with $2N$ equations that are linear in the $4N$ unknown quantities σ_i and γ_i. In order to make the system determinate the source and vortex densities on opposite panels on the upper and lower surfaces are prescribed to be equal. The $2N$ unknown quantities may then be determined by standard methods from the $2N$ equations.

The method described above has proved to be a powerful method in practice, and has been incorporated by Butter & Williams (1980) into a method for calculating the viscous flow about high-lift aerofoils.

4. Compressible flow

In this section we show how the method described in §3 may be extended to subcritical compressible flow, where its value becomes apparent in applications to the flow past multi-element configurations.

The exact methods outlined above, based upon conformal transformations, that have been used for incompressible-flow problems are no longer available. Sells (1968), Garabedian & Korn (1971) and Suddhoo (1985) all present finite-difference solutions of (2.1) for compressible flow past a single lifting aerofoil. Suddhoo follows Sells by mapping the flow field to the inside of a circle which is then the computational domain. He extends this method for a two-element configuration by mapping the computational domain onto the annulus between two circles, which themselves represent the boundaries of the two aerofoils, and his calculations are not limited to subcritical flow. The mapping technique overcomes the difficulty of devising a suitable computational mesh, since in a circular domain polar coordinates may be conveniently used. Although Suddhoo has demonstrated that his method may be extended to the symmetric flow past three in-line cylinders it is not at present clear that more than two lifting elements can be introduced. The difficulties of grid generation for multi-element configurations are overcome by D. A. King (1984, private communication, British Aerospace, Hatfield) who uses a finite-element method that is also capable of handling flows in the supercritical regime. We note that by its very nature a panel method is not restrictive in the sense that, apart from the obvious additional computational effort, it may be used to calculate the flow past a multi-element configuration in the same manner as for a single element.

Since the compressible-flow problem is nonlinear, an iterative method of solution has to be adopted, and this is outlined schematically in (2.4). However, before this can be implemented it is necessary to find the fundamental solution of (2.5), with $\rho = \rho(x, y)$ assumed known. Such a solution is the analogue of (3.2), and a distribution of such singular solutions over the boundary C, which may consist of one or more elements, is used to represent the solution of our boundary-value problem.

For subcritical flow (2.5) remains elliptic. Vekua (1967) and Bergman (1969) have addressed themselves to the problem of determining the fundamental solution of second-order, linear, elliptic partial differential equations. Their methods lead to an integral representation of the solution, whereas, as we see below, our approach leads to an integral equation for the solution. In the forthcoming paper Hill & Porter (1986) make a detailed examination of the relationship between the three methods.

Guided by the work of Vekua and Bergman, we first analytically continue the variables x, y into the complex plane, and introduce new independent complex variables z, w as

$$z = x + \mathrm{i}y, \quad w = x - \mathrm{i}y. \tag{4.1}$$

If we then denote the analytic continuation of any variable by a caret we have

$$\hat{\Phi}(z, w) = \Phi(\tfrac{1}{2}(z+w), -\tfrac{1}{2}\mathrm{i}(z-w)), \tag{4.2}$$

as the analytic continuation of Φ and then, using (4.1), the analytic continuation of (2.5) may be written as

$$\frac{\partial^2 \hat{\Phi}}{\partial z\, \partial w} + \frac{\partial}{\partial z}(\log \hat{\rho}) \frac{\partial \hat{\Phi}}{\partial z} + \frac{\partial}{\partial w}(\log \hat{\rho}) \frac{\partial \hat{\Phi}}{\partial w} = 0. \tag{4.3}$$

Finally, if we write

$$\hat{\Phi}(z, w) = \hat{\rho}^{-\frac{1}{2}} F(z, w), \tag{4.4}$$

then, with

$$h = \hat{\rho}^{-\frac{1}{2}} \frac{\partial^2 \hat{\rho}^{\frac{1}{2}}}{\partial z\, \partial w}, \tag{4.5}$$

the equation for F is

$$\frac{\partial^2 F}{\partial z\, \partial w} - hF = 0, \tag{4.6}$$

and it is the fundamental solution of (4.6) that we now seek.

From (4.6) we have

$$F(z,w) = \alpha(z) + \beta(w) + \int^{z} \int^{w} h(t,\tau)\, F(t,\tau)\, \mathrm{d}\tau\, \mathrm{d}t, \tag{4.7}$$

where α, β are arbitrary functions. Noting the form of the fundamental solution (3.2) for incompressible flow, we choose $\alpha(z) = \log(z-\delta), \beta(w) = 0$, where δ is a complex constant and, if the complex conjugate is denoted by an overbar, (4.7) is written as

$$F(z,w;\delta,\bar{\delta}) = \log(z-\delta) + \int_{\delta}^{z} \int_{\bar{\delta}}^{w} h(t,\tau)\, F(t,\tau;\delta,\bar{\delta})\, \mathrm{d}\tau\, \mathrm{d}t, \tag{4.8}$$

which is a Volterra integral equation for F. Writing $w = \bar{z}$, we then have

$$F(z,\bar{z};\delta,\bar{\delta}) = \log R + \mathrm{i}\theta + \int_{\delta}^{z} \int_{\bar{\delta}}^{\bar{z}} h(t,\tau)\, F(t,\tau;\delta,\bar{\delta})\, \mathrm{d}\tau\, \mathrm{d}t. \tag{4.9}$$

If $\rho = 1$, corresponding to incompressible flow, then $h = 0$ and $F(z,\bar{z};\delta,\bar{\delta})$ in (4.9) is immediately identified with (3.2). The double integral in (4.9) may therefore be interpreted as a correction, due to compressibility effects, to the fundamental solution for incompressible flow (3.2). The solution of the Volterra equation (4.8) is described in detail by Hill & Porter (1986); here we give a brief outline of the method.

Because of the logarithmic singularity that appears explicitly in (4.8) we find it convenient to write

$$F(z,w;\delta,\bar{\delta}) = \log(z-\delta) + G(z,w;\delta,\bar{\delta}), \tag{4.10}$$

and to solve the equation for G, namely

$$G(z,w;\delta,\bar{\delta}) = \int_{\delta}^{z} \int_{\bar{\delta}}^{w} h(t,\tau) \log(t-\delta)\, \mathrm{d}\tau\, \mathrm{d}t + \int_{\delta}^{z} \int_{\bar{\delta}}^{w} h(t,\tau)\, G(t,\tau;\delta,\bar{\delta})\, \mathrm{d}\tau\, \mathrm{d}t. \tag{4.11}$$

For the method of solution we refer to the schematic diagram, figure 2, in which a 'rectangle' is shown in the (z,w)-plane whose diagonal PQ represents the real line $z = \bar{w}$. In terms of the solution of the physical problem under consideration the point $(\delta,\bar{\delta})$ represents the point $\boldsymbol{p}$ on one of the elements in the flow field at which we apply the boundary condition (2.3*b*), whilst the point $(z,\bar{z})$ represents a point $\boldsymbol{q}$ on the boundary as, for example, in (3.3) or (3.4). The real line $z = \bar{w}$ then represents a path that connects $\boldsymbol{p}$ and $\boldsymbol{q}$. It is convenient, although not necessary, to let the path coincide with one of the boundaries of the flow. However, when $\boldsymbol{p}$ and $\boldsymbol{q}$ lie on different elements of a multi-element configuration this is not possible, and part of the path must then lie in the flow field itself. With reference to (4.11) we have in figure 2 $G = 0$ along PA and PB and we determine G at Q from a numerical evaluation of (4.11) as follows. Suppose that the rectangle is divided into a rectangular grid. Further suppose that the solution has been determined at all grid points within, and along, the boundary of the rectangle $PA'Q'B'$ except at the point Q' itself. Then, a numerical representation of (4.11) over this rectangle provides an explicit estimate for G at Q'. The solution may be continued in this manner up to the point Q for all points $\boldsymbol{q}$ on the boundary. Note from (4.5) that the analytic continuation of the density ρ is required when solving (4.11). This is obtained as follows. With the density updated from (2.4*b*) it is continued analytically by first forming a series of subcovers in the neighbourhood of all points along the line PQ, and then in a similar manner extending this to the whole of the rectangular domain $PAQB$. It may be noted that the error incurred in series truncation is comparable with that associated with the implemen-

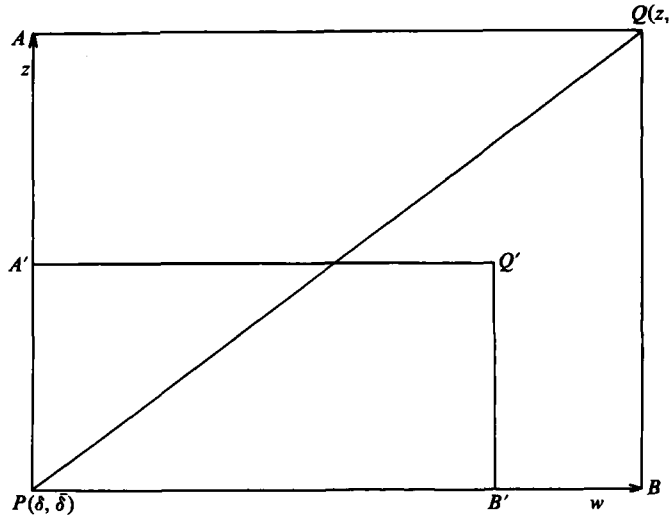

FIGURE 2. Domain of integration for the function G in (4.12).

tation of the panel method. This procedure leads to a unique analytic continuation, and for further details of it reference may be made to Hill (1983). Finally, we determine F from (4.10) and write

$$F = \rho^{\frac{1}{2}}(\Psi + \mathrm{i}\Theta) \tag{4.12}$$

so that Ψ and Θ are now the analogues, for compressible flow, of (3.2). The solution of the boundary-value problem, as for incompressible flow, is completed by noting that the analogue of (3.4) is

$$\rho(\boldsymbol{p})\frac{\partial \Phi(\boldsymbol{p})}{\partial n_p} = \frac{\partial \Phi_\infty(\boldsymbol{p})}{\partial n_p} + \pi\rho(\boldsymbol{p})^{\frac{1}{2}}\sigma(\boldsymbol{p}) + \rho(\boldsymbol{p})\int_C \sigma(\boldsymbol{q})\frac{\partial \Psi}{\partial n_p}(\boldsymbol{p}-\boldsymbol{q})\,\mathrm{d}q + \rho(\boldsymbol{p})\int_C \gamma(\boldsymbol{q})\frac{\partial \Theta}{\partial n_p}(\boldsymbol{p}-\boldsymbol{q})\,\mathrm{d}q. \tag{4.13}$$

The determination of σ, γ follows, exactly as in the case of incompressible flow, from (2.3b) and (4.13).

In the iterative method (2.4) we first set $\rho \equiv 1$ so that Ψ, Θ are as in (3.2). We then solve the Fredholm integral equation, derived from (2.3b) and (4.13), for the source and vortex strengths σ and γ. From (4.13) and its analogue for $\partial\Phi/\partial s$ where (s, n) are orthogonal, we may obtain from (2.4b) a new estimate for the density ρ which is then analytically continued into the complex (z, w)-plane in the manner described above. With h determined as in (4.5) we solve the Volterra integral equation (4.11) for G and so, from (4.10) and (4.12), obtain new estimates for Ψ and Θ. This process is then continued until convergence is achieved according to some pre-set criterion. The convergence properties of the iterative scheme are discussed in the next section.

5. Convergence

In discussing the convergence properties of the numerical procedure outlined in §4, we begin by considering the linearization (2.4) and establish the following:

THEOREM. *Let Φ^{i+1} be the solution of* (2.4a) *with $\rho^i = B(\Phi^i)$ given by* (2.4b). *Then if for some i the maximum local Mach number $M^i \leqslant 1$,* (2.4a) *is elliptic, and hence for*

a given circulation has a unique solution subject to (2.3). *Moreover, if this solution is such that* $M^{i+1} \leqslant L < 1$ *for all* x, y, *then*

$$\|\Phi^{i+1} - \Phi\| \leqslant L^2 \|\Phi^i - \Phi\|, \tag{5.1}$$

where $\|u\|^2 = \int_\Omega \rho |\nabla u|^2 \, \mathrm{d}\Omega$, *and* Ω *is the region exterior to* C.

This theorem provides the basis for the iterative procedure.

Proof. From the definition of the norm we have, using (2.4a), (2.1) and Green's first identity,

$$\|\Phi^{i+1} - \Phi\|^2 = \int_\Omega (\rho^i - \rho) \nabla\Phi^{i+1} \cdot (\nabla\Phi - \nabla\Phi^{i+1}) \, \mathrm{d}\Omega. \tag{5.2}$$

Use of Bernoulli's equation (2.2) for ρ and ρ^i gives after some manipulation, as in Hill (1983),

$$\rho^i \geqslant \rho \{1 + M_1^2 (\rho^i)^{1-\gamma} \nabla\Phi^i \cdot \nabla(\Phi - \Phi^i)\}. \tag{5.3}$$

Then (5.2) becomes, using the Cauchy–Schwarz inequality together with (5.3),

$$\|\Phi^{i+1} - \Phi\|^2 \leqslant \int_\Omega \rho M_1^4 (\rho^i)^{2-2\gamma} \, |\nabla\Phi^i|^2 \, |\nabla\Phi^i - \nabla\Phi|^2 \, |\nabla\Phi^{i+1}|^2 \, \mathrm{d}\Omega. \tag{5.4}$$

Further use of Bernoulli's equation gives

$$\begin{aligned} (\rho^i)^{1-\gamma} |\nabla\Phi^{i+1}|^2 &\leqslant (\rho^{i+1})^{1-\gamma} |\nabla\Phi^{i+1}|^2 \quad \text{if} \quad |\nabla\Phi^i| < |\nabla\Phi^{i+1}|, \\ &\leqslant (\rho^i)^{1-\gamma} |\nabla\Phi^i|^2 \quad \text{if} \quad |\nabla\Phi^i| \geqslant |\nabla\Phi^{i+1}|, \end{aligned} \tag{5.5}$$

so that substitution in (5.4), with the identity $M_1 |\nabla\Phi^i| = (\rho^i)^{\frac{1}{2}(\gamma-1)} M^i$, shows that, if $M^i \leqslant L < 1$, then

$$\|\Phi^{i+1} - \Phi\| \leqslant L^2 \|\Phi^i - \Phi\|, \tag{5.6}$$

and the theorem is established.

The numerical solution of the Volterra equation (4.11) has been discussed in detail by Hill (1983), and Hill & Porter (1986). Here we simply state the result:

$$|G(z, \bar{z}; \delta, \bar{\delta}) - \tilde{G}(z, \tilde{z}; \delta, \bar{\delta})| = O(k_1^2), \tag{5.7}$$

where $\tilde{G}$ is the numerical approximation to the solution G of (4.11) and k_1 is a typical grid size in the mesh on the rectangle of figure 2. In practice this is taken to be comparable with the panel length in the solution of the Fredholm integral equation (4.13).

As far as the numerical solution of (4.13) itself is concerned, we note the result (see Wendland 1985) that, if $u(s)$ is a solution of

$$u(s) = f(s) + \int_C K(s, t) \, u(t) \, \mathrm{d}t, \tag{5.8}$$

and K is weakly singular, then

$$\|u - u_n\|_2 = O(k_2^2). \tag{5.9}$$

In (5.9) the L_2 norm is intended, and u_n is the approximation to u obtained from a numerical evaluation of (5.8) in which k_2 is the maximum panel length.

The results of this section show that, for subsonic flow, the iterative numerical procedure outlined in earlier sections will converge to a solution with an error that is of the order of the square of the maximum panel length in the discretization of C. The number of iterations that are required in practice depends upon the particular flow under consideration. However, in most cases we have found it to be about 10.

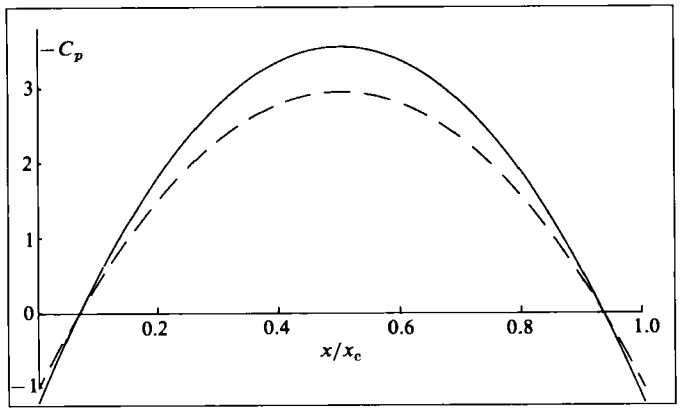

FIGURE 3. Pressure distribution over the upper surface of a circular cylinder for $M_1 = M_c = 0.4$ (——); $M_1 = 0$ (– – –).

6. Calculated results

We have used the method outlined in §4 to calculate the subcritical flow past representative single- and multi-element configurations with varying degrees of complexity. For symmetric shapes, with which we are initially concerned, it should be noted that $\gamma(q) \equiv 0$ in (4.13).

We consider first the simplest case of all, namely that of flow past a single circular cylinder. The classical Rayleigh–Janzen expansion (see for example Van Dyke 1975) predicts a critical Mach number M_c at which flow becomes sonic, as 0.398. Williams (1979), using a finite-element method, gives $M_c = 0.400$, a value with which we agree when using 160 panels in all. In figure 3 we show the pressure coefficient $C_p = (p-p_1)/\frac{1}{2}\rho_1 U_1^2$ over the upper half of the cylinder for $M_1 = M_c$. Also included for comparison is the pressure distribution for incompressible flow.

Our second example is the symmetric flow past two in-line circular cylinders. These are placed with their centres at a distance of three radii apart. For incompressible flow an exact solution is available which may be obtained by the method of Williams (1973). For compressible flow Suddhoo (1985) maps the two circles to the boundaries of an annulus of circular cross-section and calculates the flow in this transformed plane by finite-difference methods on a polar grid. Our panel method of solution, now using 80 panels on each element, is implemented exactly as for a circular cylinder with the exception that the path of integration in the solution of the Volterra equation (4.11) may now span the fluid region between the two cylinders. In such cases we have always chosen the shortest path between the two elements of the configuration that are involved. The pressure distribution over the upper surfaces of the two cylinders is shown in figure 4 for the case $M_1 = M_c = 0.43$. We again include the incompressible result for comparison. In those cases where we have been able to make a comparison with the finite-difference calculations of Suddhoo (1985) we record agreement in which the solutions are graphically indistinguishable.

One of the earliest compressible-flow calculation methods for a single aerofoil is that due to Sells (1968) who maps the flow field to the interior of a circle whose boundary is the aerofoil surface. One of the examples given by Sells is the non-lifting symmetric flow past the RAE 101 aerofoil section with $M_1 = 0.7457$ for which he finds the maximum local Mach number to be 0.991. For this value of M_1, and using 160 panels,

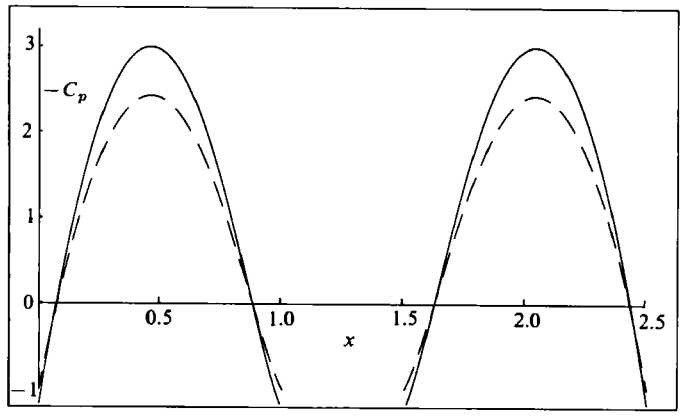

FIGURE 4. Pressure distribution over the upper surfaces of two in-line circular cylinders for $M_1 = M_c = 0.43$ (——); $M_1 = 0$ (– – – –).

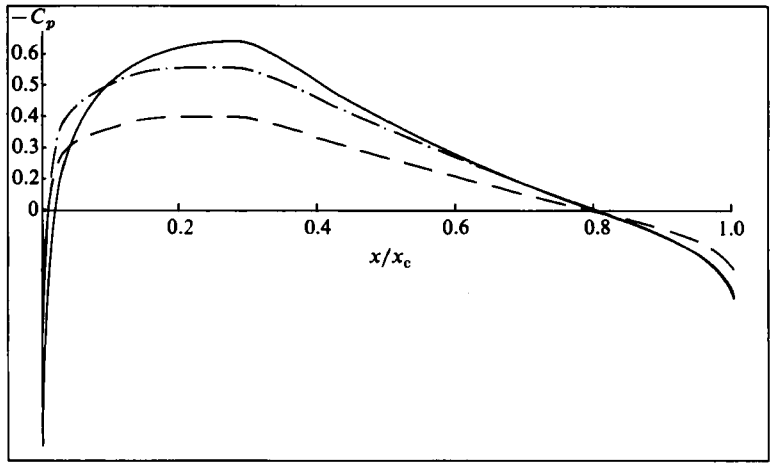

FIGURE 5. Pressure distribution for symmetric flow over the upper surface of the RAE 101 aerofoil section for $M_1 = 0.7457$ (——); $M_1 = 0$ (– – – –). Also shown is the Prandtl–Glauert result for $M_1 = 0.7457$ (–·–·–·–).

we find this local maximum to be 0.9905. Figure 5 shows the pressure distribution over the aerofoil surface, for $M_1 = 0.7457$, and we note that the results of Sells are identical on this scale. In figure 5 the incompressible-flow solution is again included for comparison and also, for this case only, we show the pressure distribution predicted by the Prandtl–Glauert approximation. This is believed to give a good approximation if the local Mach number does not exceed 0.6. In the case under consideration, in which the flow is almost critical, the Prandtl–Glauert approximation is seen to be quite inadequate.

Another popular test case is the NACA 0012 aerofoil section. The pressure distribution over the upper and lower surfaces, using 160 panels in each case, for two different incidences is shown in figure 6. For each case the free-stream Mach number M_1 is chosen such that the flow conditions are almost critical. The higher-incidence case, shown in figure 6 (*a*), is a particularly severe test because of the very high loading

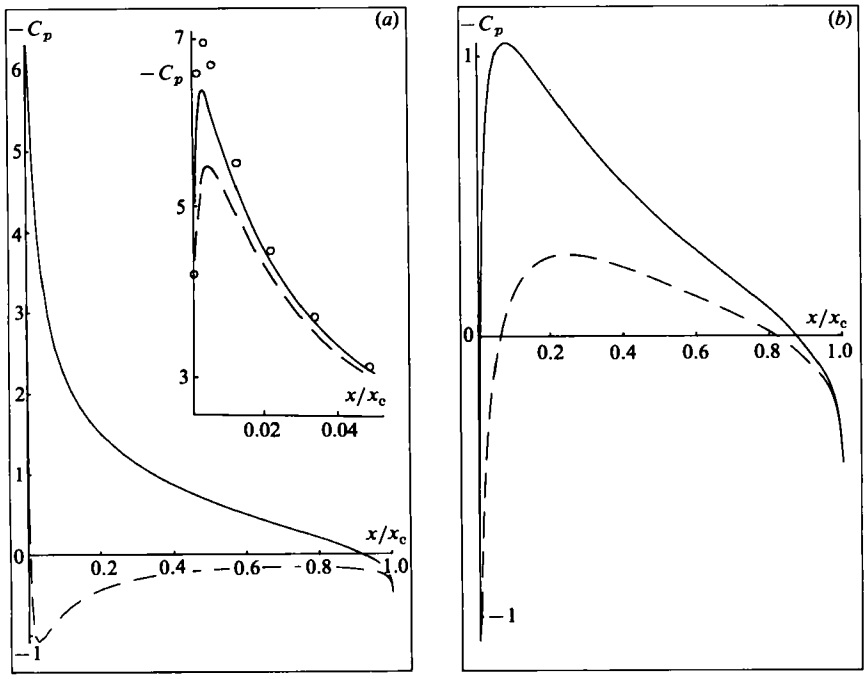

FIGURE 6. (*a*) Pressure distribution over the NACA 0012 aerofoil section; upper surface (——), lower surface (– – – –). $M_1 = 0.3$, incidence $\alpha = 10°$. The inset compares the suction peak using 80 panels (– – – –) and 160 panels (——) with a solution using the method of Garabedian & Korn (○). (*b*) As (*a*) with $M_1 = 0.63$, $\alpha = 2°$.

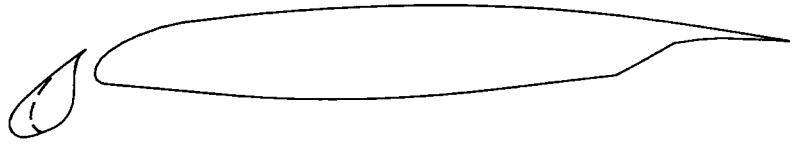

FIGURE 7. The National High-Lift aerofoil section. The slat heel, shown as – – – –, is enveloped by a vortex sheet.

on the upper surface at the leading edge of the aerofoil. We have made a comparison of our results for each of these cases with solutions by the method of Garabedian & Korn (1971), kindly supplied by Dr R. C. Lock, in which there are also 160 grid points on the aerofoil surface. For the case shown in figure 6(*b*) the results are graphically indistinguishable. This is true also of figure 6(*a*) except in the neighbourhood of the suction peak. It is in the neighbourhood of sharp, high suction peaks that we might expect differences between different solution methods, and we highlight the difference in this case on the inset to figure 6(*a*). We see that panel refinement leads to closer agreement with the finite-difference solution, and we record a difference of just over 2 % in the lift coefficient. D. A. King (1985, private communication, British Aerospace, Hatfield) has developed a finite-element technique for compressible flow past multi-element aerofoils and when applied to the NACA 0012 the results are graphically indistinguishable from those presented in figure 6.

The first multi-element aerofoil configuration for which we present results is that associated with the National High-Lift Programme, and is shown in figure 7. It was

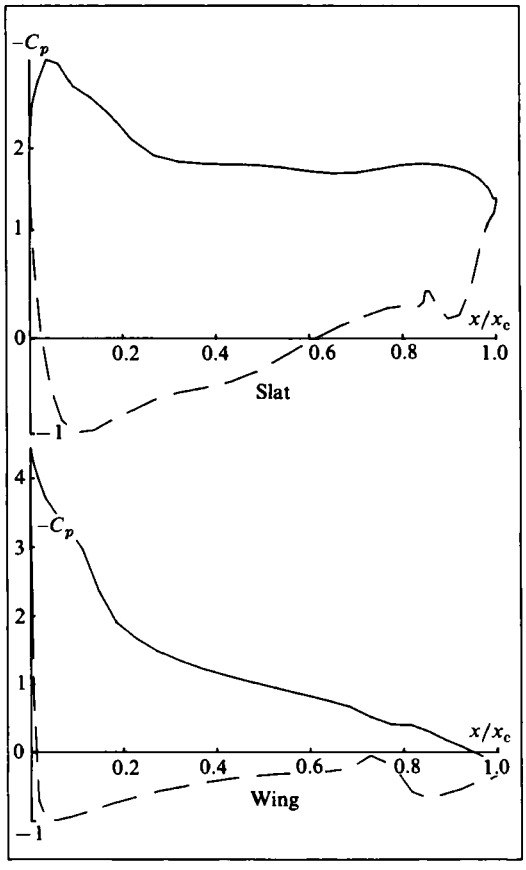

FIGURE 8. Pressure distribution over the slat and main aerofoil for the National High-Lift wing. For each element —— denotes upper-surface distribution; ----, lower-surface. $M_1 = 0$, $\alpha = 15°$.

originally in three-element form, but the flap has been omitted although the cove at the rear of the main aerofoil is retained. Also, in this case flow separation across the slat heel has been modelled by a vortex sheet. The solutions that we present in figures 8 and 9, for $M_1 = 0$ and 0.2 respectively, have been obtained using 60 panels on each element of the configuration. In figure 9, for which $M_1 = 0.2$, the maximum local Mach number in the flow field is 0.73. At this free-stream Mach number significant compressibility effects are apparent only over the leading edges of the upper surfaces of the elements. (Note that for this value of M_1, $C_p = -16.314$ when the flow becomes critical.) A comparison between the present results, and those obtained from the finite-element method under development at British Aerospace by King gives agreement to within graphical accuracy except at the suction peaks, for which we make a more detailed comparison in table 1. On the main aerofoil an unexplained trend is the magnitude of the suction peak, which decreases with Mach number in the finite-element method but increases in the present method.

Finally, we consider the three-element configuration shown in figure 10. This configuration has been devised by Suddhoo (1985) from a conformal transformation of three circles, and an exact solution is given by him for incompressible flow. Our results, shown in figures 11 and 12 for $M_1 = 0$ and 0.15 respectively, have been obtained using 60 panels on each element of the configuration. For the higher

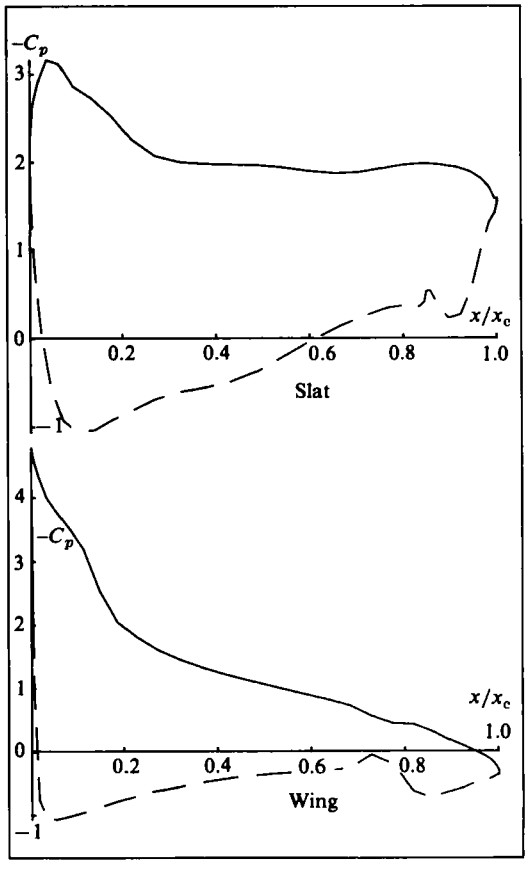

FIGURE 9. As figure 8; $M_1 = 0.2$, $\alpha = 15°$.

	Slat		Main wing	
M_1	K	P	K	P
0.0	3.05	2.95	5.6	4.5
0.1	3.07	3.03	5.5	4.6
0.2	3.14	3.15	5.4	4.8

TABLE 1. A comparison between the suction peaks on the slat and the main aerofoil, for the configuration shown in figure 7, using the finite-element (K) and present (P) methods

free-stream Mach number the maximum local Mach number that is achieved is 0.53 and as a consequence there are no significant effects due to compressibility. (We may note that, for this value of M_1, $C_p = -29.419$ when the flow becomes critical.) Again we report excellent agreement with the finite-element results of King except in the neighbourhood of the suction peaks, which are compared in table 2. In that table we are also able to include the exact result of Suddhoo for incompressible flow. We again note the opposing trend, as the Mach number increases, in maximum suction on the two rear elements.

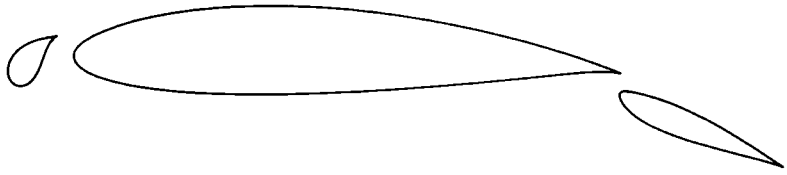

FIGURE 10. The Suddhoo (1985) three-element aerofoil.

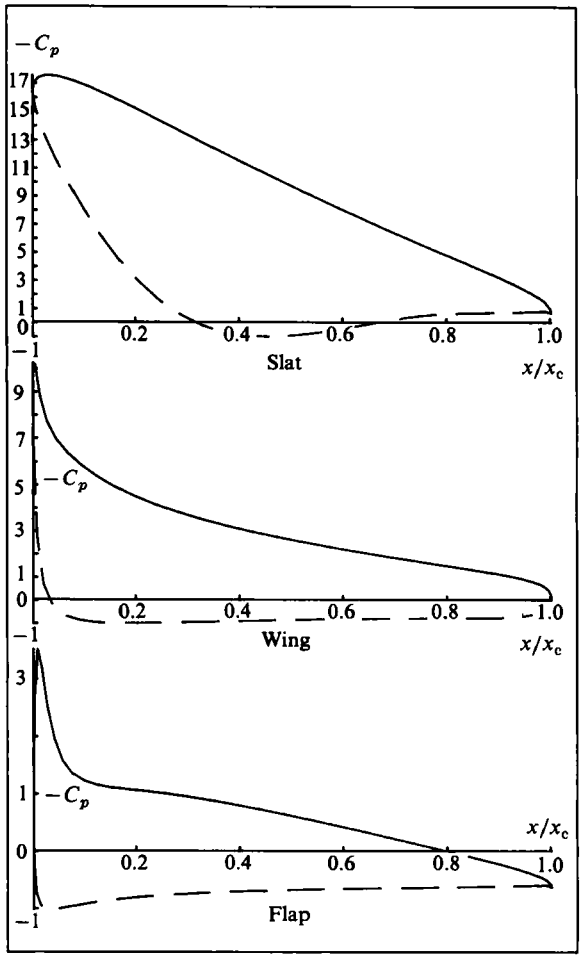

FIGURE 11. Pressure distribution over three elements of the Suddhoo configuration. For each element —— denotes upper-surface distribution; – – – –, lower-surface. $M_1 = 0$, $\alpha = 20°$.

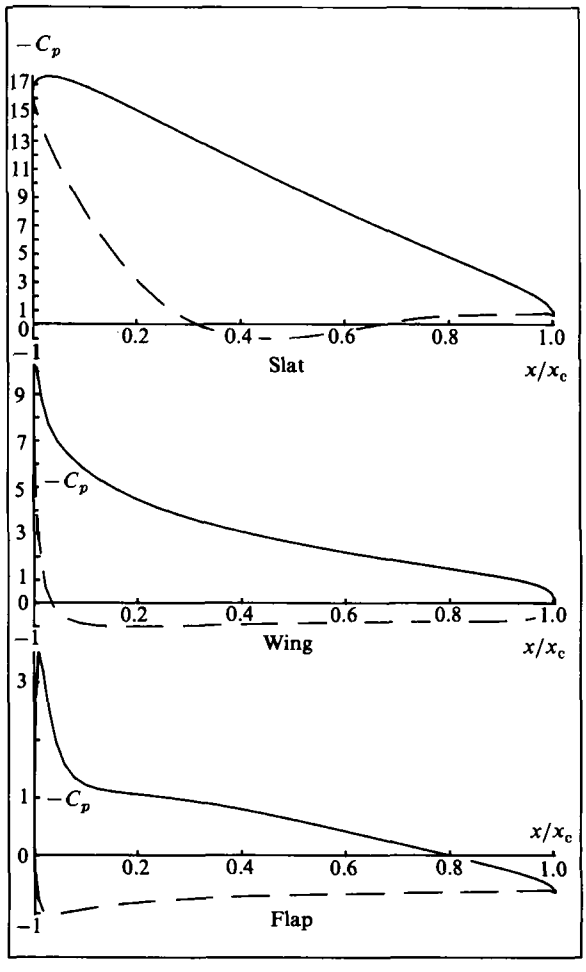

FIGURE 12. As figure 11; $M_1 = 0.15$, $\alpha = 20°$.

	Slat			Main wing			Flap		
M	K	P	S	K	P	S	K	P	S
0.0	17.5	17.1	17.4	11.9	11.02	11.5	3.3	3.4	3.7
0.1	17.8	17.5	—	11.6	11.3	—	3.2	3.5	—
0.15	18.4	18.1	—	11.2	11.8	—	3.2	3.6	—

TABLE 2. A comparison between the suction peaks on the slat, the main aerofoil and the flap, for the configuration shown in figure 10, using the finite-element (K) and present (P) methods. The exact result of Suddhoo for incompressible flow is also shown (S).

7. Conclusions

In this paper we have presented a panel method for the solution of subcritical plane potential flow past one or more finite bodies. The method is an extension of panel methods that are familiar for incompressible flow. Although compressibility effects lead inevitably to an additional computational effort, the method possesses all the flexibility of those used for incompressible flow. In particular, no restrictions are placed upon the method, in principle, when multi-element aerofoil configurations, with two or more elements, are encountered. The effectiveness of the method has been demonstrated in several test cases having varying degrees of complexity.

Financial support for this project for SERC, within the framework of the BAe/RAE high-lift wing initiative, is gratefully acknowledged, as are helpful discussions with R. C. Lock, J. H. B. Smith, B. R. Williams of RAE and D. A. King of BAe (Hatfield). We are particularly indebted to B. R. Williams for supplying details of all the aerofoil sections used.

REFERENCES

BERGMAN, S. 1969 *Integral Operators in the Theory of Linear Partial Differential Equations.* Springer.

BUTTER, D. J. & WILLIAMS, B. R. 1980 In *Proc. AGARD Conf. 291, Colorado Springs, Paper No.* 25.

GARABEDIAN, P. R. & KORN, D. G. 1971 *Commun. Pure Appl. Maths* **24**, 841.

HESS, J. L. 1973 *Comp. Meth. Appl. Mech. Engng* **2**, 1.

HESS, J. L. & SMITH, A. M. O. 1966 *Prog. Aero. Sci.* **8**, 1.

HILL, M. G. 1983 The boundary-integral method for subsonic compressible flow. Ph.D. thesis, Reading University.

HILL, M. G. & PORTER, D. 1986 The numerical determination of fundamental solutions. *IMA J. Numer. Anal.* (submitted).

NEWLING, J. C. 1977 *Hawker Siddeley Aviation Rep.* HSA-MAE-R-FDM-0007.

OSKAM, B. 1985 Transonic panel method for the full potential equation applied to multi-component airfoils. *AIAA J.* (to be published).

SELLS, C. C. 1968 *Proc. R. Soc. Lond.* A **393**, 377.

SUDDHOO, A. 1985 Inviscid compressible flow past multi-element aerofoils. Ph.D. thesis, Manchester University.

VAN DYKE, M. D. 1975 *Perturbation Methods in Fluid Mechanics.* Parabolic Press.

VEKUA, I. N. 1967 *New Methods for Solving Elliptic Equations.* North-Holland.

WENDLAND, W. L. 1985 In *Proc. MAFELAP 1984* (ed. J. R. Whiteman), pp. 193–227. Academic.

WILLIAMS, B. R. 1973 *Aero. Res. Counc. R. & M.* 3717.

WILLIAMS, B. R. 1979 An investigation of the flow around multiple-element wings by the finite-element method. Ph.D. Thesis, Reading University.